https://doi.org/10.5194/egusphere-2025-4626
Preprint. Discussion started: 14 November 2025

Integrating MethaneAIR aircraft and TROPOMI satellite observations in the Integrated Methane Inversion (IMI) to optimize methane emissions

Jack H. Bruno[1], Daniel J. Jacob[1,2], Xiaolin Wang[2], Melissa P. Sulprizio[2], Lucas A. Estrada[2], Daniel J. Varon[2,3], Steven C. Wofsy[2,4], Mark Omara[4], Ritesh Gautam[4]
[1]Department of Earth and Planetary Sciences, Harvard University, Cambridge, MA 02138, USA
[2]School of Engineering and Applied Sciences, Harvard University, Cambridge, MA 02138, USA
[3]Department of Aeronautics and Astronautics, Massachusetts Institute of Technology, MA 02139, USA
[4]Environmental Defence Fund, New York, NY, USA

Correspondence to: Jack H. Bruno (jackbruno@g.harvard.edu)

Abstract. The MethaneAIR aircraft remote sensing instrument observes methane dry air column mixing ratios (X_{CH4}) over ~100×100 km^2 scenes with sub-km resolution, from which methane emissions can be inferred by inverse analysis with an atmospheric transport model. It emulates the MethaneSAT satellite instrument launched in March 2024 to quantify emissions from oil/gas production regions. We show here how the single day MethaneAIR observations can be integrated with the global continuous but relatively coarse and sparse observations from the TROPOMI satellite instrument into a common Integrated Methane Inversion (IMI) platform for optimizing methane emissions. The IMI, originally designed for TROPOMI, is used here with 12×12 km^2 spatial resolution and lognormal error probability density functions (PDFs) for prior estimates. Application to two scenes in oil/gas production basins of the western US shows remarkable consistency between independent MethaneAIR (single day) and TROPOMI (monthly) inversions including for emission hotspots, with some differences that may reflect temporal variability of emissions. The IMI is able to optimize emissions even when starting from a very poor prior estimate. Using TROPOMI inversion results as prior estimate improves the MethaneAIR inversions by correcting emissions upwind of the MethaneAIR observation scenes and by adding information to the original prior estimate.

1 Introduction

Methane is a potent greenhouse gas responsible for 30% of global warming since pre-industrial time (Szopa et al., 2021). Emissions originate from a range of anthropogenic source sectors that are difficult to quantify including livestock, waste, oil/gas, coal mining, and rice agriculture. Atmospheric observations of methane concentrations from surface sites, aircraft, and satellites can improve estimates of methane emissions by inverse analyses that use an atmospheric chemical transport model (CTM) as forward model to relate emissions to concentrations. These different observation platforms provide emission information on different scales and integrating that information across scales is a challenge. Here, we show how information from the TROPOMI satellite instrument can be compared and combined with information from the MethaneAIR aircraft remote sensing instrument through the Integrated Methane Inversion (IMI). MethaneAIR is the airborne version of the MethaneSAT satellite instrument launched in March 2024, and the work presented here lays the foundation for integrating

https://doi.org/10.5194/egusphere-2025-4626
Preprint. Discussion started: 14 November 2025

TROPOMI and MethaneSAT in a common operational inversion framework. Contact with MethaneSAT was lost in June 2025, but there is a substantial data archive from its operational lifetime upon which this work can be applied.

The TROPOMI instrument launched in October 2017 provides continuous global daily mapping of dry air column methane mixing ratios (X_{CH4}) at nadir pixel resolution of 5.5×7 km^2 (Lorente et al., 2021). It uses a full-physics retrieval for solar backscatter in the 2.3 μm methane absorption band, with a success rate averaging only 3% limited by clouds, heterogeneous and dark surfaces, and aerosols (Lorente et al., 2021). Inversions of TROPOMI data have been used extensively to quantify methane emissions on regional to continental scales (Chen et al., 2022; Liang et al., 2023; Shen et al., 2023; Hemati et al., 2024) but are limited to 10–100 km spatial resolution and weekly–monthly temporal resolution because of limitations on coverage and precision (Jacob et al., 2022). MethaneSAT observes 200×200 km^2 targets with 140×400 m^2 pixel resolution, and similarly retrieves X_{CH4} but in the 1.6 μm band where high precision can be achieved with the CO_2 proxy method (Chan Miller et al., 2024). MethaneSAT can observe approximately 30 targets per day. MethaneAIR emulates MethaneSAT but with much finer pixel resolution (Chan Miller et al., 2024). Both provide much finer information than TROPOMI for their days of observations, but TROPOMI provides a wider spatial and temporal context. The problem is how to properly compare and combine the information from these different platforms.

The IMI (Varon et al., 2022; Estrada et al., 2025) is a user-friendly, cloud-based software tool designed for Bayesian analytical inversion of TROPOMI data with the GEOS-Chem CTM driven by global NASA GEOS assimilated meteorological data as forward model (https://carboninversion.com). The IMI has been widely used to quantify methane emissions on regional scales (Baray et al., 2023; Chen et al., 2023; Nathan et al., 2024; Hemati et al., 2024; Hancock et al., 2025) and at up to weekly resolution (Varon et al., 2023). The standard version of the IMI operates at up to 25-km resolution with 3-hourly meteorological fields, but Wang et al. (2025) recently developed a 12×12 km^2 version using hourly meteorological fields.

Here we show how the IMI can be used as a common platform for inversion of TROPOMI and MethaneAIR data, exploiting the new 12×12 km^2 capability. We address the challenge of combining within the same inversion system the temporally and spatially limited but precise information from MethaneAIR with the continuous but sparser and lower precision information from TROPOMI. The IMI framework enables the use of TROPOMI to provide spatial context (boundary conditions) and temporal context (monthly mean versus daily snapshot) for the MethaneAIR inversion. It also provides an operational capability that can be deployed anywhere in the world. We demonstrate the capability for two MethaneAIR scenes in oil/gas production regions of the western USA. Our work paves the way for integrating MethaneSAT and comparable satellite instruments such as GOSAT-GW (Miura et al., 2023) into the IMI.

https://doi.org/10.5194/egusphere-2025-4626
Preprint. Discussion started: 14 November 2025

2 Data and Methods

2.1 MethaneAIR

The MethaneAIR instrument consists of two Offner spectrometers covering the 1237-1319 nm and 1592-1697 nm wavelength bands at 0.28 nm full-width-at-half-maximum resolution and 0.1 nm spectral sampling (Chan Miller et al., 2024). The first band is used to retrieve the O_2 column as a measure of the total air column and to reject cloudy pixels. The methane dry air column mixing ratio X_{CH4} is then retrieved in the second band using the CO_2 proxy method to correct for light path including scattering by aerosols, clouds outside the scene, and reflectivity of the surface (Frankenberg et al., 2005; Krings et al., 2011, Chan Miller et al. 2024). The retrieval fits the difference of the vertical profile of methane mixing ratios $\boldsymbol{z}$ at 19 vertical levels with a prior estimate $\boldsymbol{z_A}$ from the TCCON GGG2020 archive (Laughner et al., 2024). The sensitivity is expressed by an averaging kernel vector $\boldsymbol{a}$ reported for the individual retrievals:

$$X_{CH4} = \boldsymbol{a}^{T}\boldsymbol{z} + (\mathbf{1} - \boldsymbol{a})^{T}\boldsymbol{z_A} \quad (1)$$

where $\mathbf{1}$ is a vector of unit values. The elements of $\boldsymbol{a}$ are near unity (>0.9) below the aircraft and ~0.4 above the aircraft.

The MethaneAIR data analyzed here are from level flights at 13 km altitude conducted in a raster pattern across ~100×100 km^2 scenes. The instrument samples in a push-broom mode along a cross-track swath of 4.5 km (Chulakadabba et al., 2023). Pixels have 4 × 20 m^2 nadir resolution separated by 5 m cross-track and 25 m along track. The single-pixel precision is 80 ppb (Chan Miller et al, 2024). The native-resolution pixels are used to detect point sources (Chulakadabba et al., 2023), and the data are otherwise co-added spatially to increase precision. Pixels with low confidence in the retrieval are flagged in the data product and removed in our analysis.

https://doi.org/10.5194/egusphere-2025-4626
Preprint. Discussion started: 14 November 2025

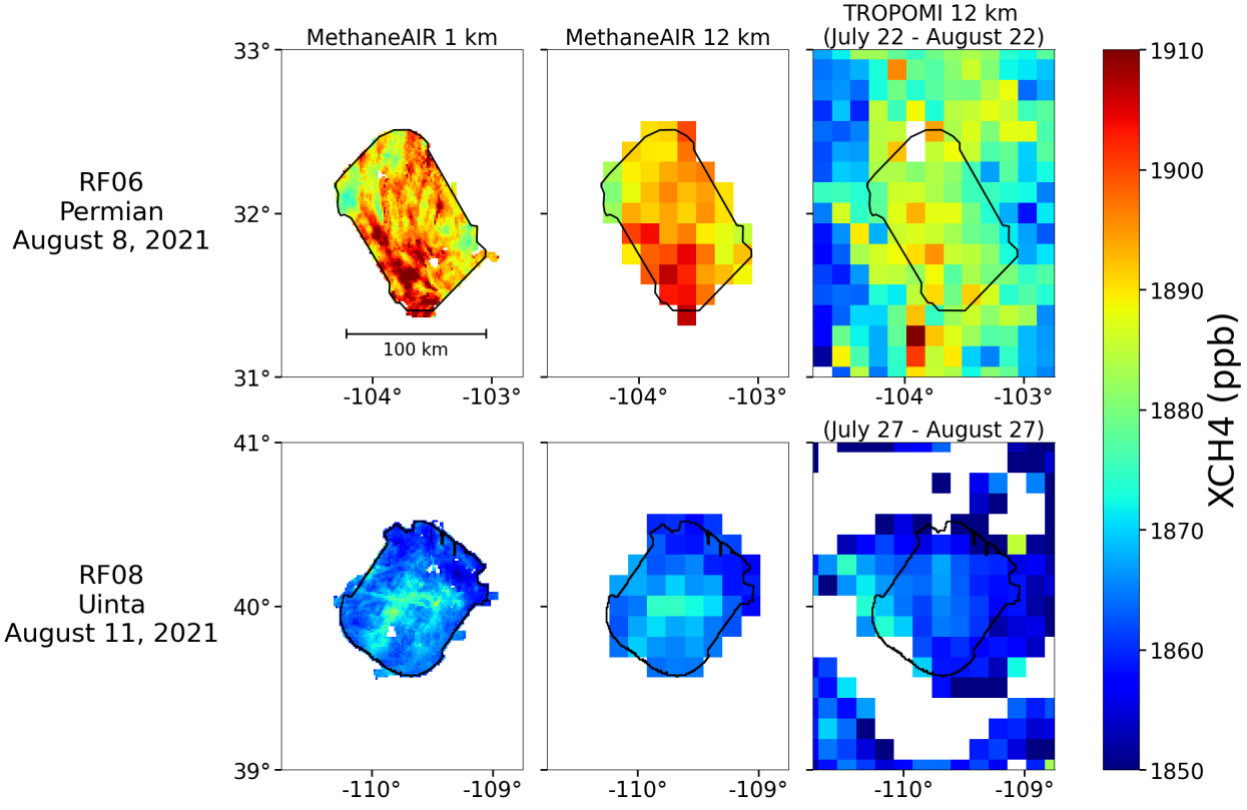

Figure 1: Methane observations from MethaneAIR research flights (RF) over the Permian (Texas, USA) and Uinta (Utah, USA) oil/gas production basins. RF06 over the Permian was conducted on August 6, 2021, and RF08 over the Uinta was conducted on August 11, 2021. Black lines delineate the MethaneAIR observation scenes. Left panels show the MethaneAIR data at 1×1 km^2 resolution. Middle panels show the MethaneAIR data aggregated to the 12×12 km^2 resolution of the inversion. Right panels show the TROPOMI data on the same 12×12 km^2 grid averaged over the monthly periods centered on each flight day (July 22-August 22 for RF06 and July 27-August 27 for RF08). White areas in the TROPOMI panels have no observations for the month. The panel edges represent the regions of interest of our inversion domain at 12×12 km^2. The full inversion domain has an additional 0.5° buffer on all sides.

Fig. 1 shows the data from the two MethaneAIR research flights (RF) analyzed in this work, together with TROPOMI data for the month centered on each flight day. RF06 observed the Delaware sub-basin of the Permian Basin in Texas (USA) on August 8, 2021, between 10 and 12 local time. This is an area within the USA's largest oil/gas field and is known for high emissions (Zhang et al., 2020, Riddick et al., 2024). The Permian has generally bright and flat surfaces enabling successful TROPOMI retrievals, as seen by the near-complete coverage for the month. RF08 observed the Uinta basin in Utah (USA) on August 11, 2021, between 10:00 and 12:00 local time. This is a smaller oil/gas production basin in a valley surrounded by mountains

https://doi.org/10.5194/egusphere-2025-4626
Preprint. Discussion started: 14 November 2025

where TROPOMI observations generally fail because of variable topography and surface reflectivity (blank areas in Figure 1). Methane enhancements are much weaker than in the Permian.

TROPOMI is on average 11 ppb lower than MethaneAIR for the Permian scene and 4 ppb lower for the Uinta scene. Chan Miller et al. (2024) previously found TROPOMI to be biased low by 5.8 ppb relative to MethaneAIR when comparing coincident observations along a transit flight from the Permian to Colorado. A mean bias is not of concern for the inversions as long as boundary conditions are consistent for each instrument. Chan Miller et al. (2024) found that MethaneAIR and TROPOMI variability were highly consistent for the coincident observations (coefficient of determination $R^2 = 0.83$, linear regression slope = 1.01), but the MethaneAIR and TROPOMI spatial variability in Figure 1 are markedly different. This may be expected from TROPOMI measuring a monthly average versus MethaneAIR measuring a single day and could reflect temporal variability in transport as well as in emissions. The effect of variability in transport is accounted for in the inversion.

2.2 The Integrated Methane Inversion (IMI)

The IMI (Varon et al., 2022; Estrada et al., 2025) optimizes a state vector $\boldsymbol{x}$ of 2-D gridded emission fluxes and boundary conditions by minimizing the Bayesian cost function $J(\boldsymbol{x})$ assuming normal error probability density functions (PDFs):

$$J(\boldsymbol{x}) = (\boldsymbol{x} - \boldsymbol{x_a})^{\mathrm{T}}\mathbf{S_a^{-1}}(\boldsymbol{x} - \boldsymbol{x_a}) + \gamma(\boldsymbol{y} - \mathbf{K}\boldsymbol{x})^{\mathrm{T}}\mathbf{S_o^{-1}}(\boldsymbol{y} - \mathbf{K}\boldsymbol{x}) \quad (2)$$

where $\boldsymbol{x_a}$ is the prior estimate, $\boldsymbol{y}$ is a vector of the observations, $\mathbf{S_a}$ is the prior error covariance matrix, $\mathbf{S_o}$ is the error covariance matrix of the observing system, $\mathbf{K} = \partial\boldsymbol{y} / \partial\boldsymbol{x}$ is the Jacobian matrix which describes the sensitivity of observations to perturbations in each element of $\boldsymbol{x}$, and $\gamma \in [0,1]$ is a regularization parameter to correct for unaccounted error covariances in the observation system (Lu et al., 2021). $\mathbf{K}$ is constructed by perturbing individual state vector elements in the GEOS-Chem CTM. The posterior estimate ($\hat{\boldsymbol{x}}$) is obtained by analytically solving for the cost function minimum.

Minimization of $J(\mathbf{x})$ in the IMI can alternatively use a lognormal error PDF for the prior emission estimates by applying equation (2) to $\ln\boldsymbol{x}$ instead of $\boldsymbol{x}$ as described by Maasakkers et al. (2019). We adopt this approach here. It prevents negative emission solutions and allows large upward corrections to better resolve the fat tail of the emission distribution such as for oil/gas facilities (Lyon et al., 2015). It can correct the spatial distribution of emissions more readily than the normal error PDF case. Minimization of the cost function is then done iteratively with a single calculation of the Jacobian (Maasakkers et al., 2019; Estrada et al., 2025; Hancock et al., 2025).

The observing system error covariance matrix $\mathbf{S_o}$ includes contributions from retrieval errors and model transport errors added in quadrature and with no error correlation between 12×12 km^2 grid cells (diagonal matrix). Chen et al. (2023) previously

https://doi.org/10.5194/egusphere-2025-4626
Preprint. Discussion started: 14 November 2025

derived a GEOS-Chem model transport error standard deviation of 5 ppb at the 25-km scale, and we assume here the same at the 12-km scale. TROPOMI error for individual retrievals is about 15 ppb (Qu et al., 2021; Shen et al., 2021; Chen et al., 2023) and we adopt that value here. When multiple TROPOMI observations for a given orbit are present in a single GEOS-Chem grid cell, we average them into a single super observation (Eskes et al., 2003). Individual TROPOMI retrievals have averaging kernel vectors near unity with little variability, and we take as averaging kernel vector for the super-observation the mean of the averaging kernel vectors for the individual observations. The reduction in retrieval error from averaging individual observations into a single super-observation is derived from the residual error method (Heald et al., 2004) as detailed by Chen et al. (2023) and formalized for the IMI by Estrada et al. (2025). It accounts for error correlation between the individual observations.

We optimize the emissions at 0.125×0.15625° spatial resolution (hereafter referred to as 12×12 km^2) by using a new IMI capability operating GEOS-Chem at that resolution with archived native-resolution hourly winds from the NASA Goddard Earth Observing System – Forward Processing (GEOS-FP), as described by Wang et al. (2025). We apply GEOS-Chem at 12-km resolution over the domains shown in Figure 1 with an additional 0.5 ° buffer region surrounding the domain. Within the buffer region we include 8 coarse resolution emission state vector elements aggregating 12×12 km^2 grid cells. Boundary conditions outside that buffer region used for the TROPOMI inversion are from a global 3-D archive of GEOS-Chem concentrations bias-corrected to match spatially (10°×12.5°) and temporally (-15 days) averaged TROPOMI data (called smoothed TROPOMI fields) as described by Estrada et al. (2025). The boundary conditions in each of the four cardinal directions are further optimized as part of the state vector. The buffer emissions and the boundary conditions are optimized with normal prior error PDFs. Prior error standard deviations are 50% for the buffer emissions and 10 ppb for the boundary conditions.

2.3 Integrating MethaneAIR observations into the IMI

Inversion of MethaneAIR observations in the IMI follows the same general procedure as inversion of TROPOMI observations but requires some specific treatments. We process the MethaneAIR data for ingestion into the IMI by averaging the individual MethaneAIR retrievals into super-observations on the GEOS-Chem 12×12 km^2 grid (Figure 1). The averaging kernels (equation 1) do not vary significantly between retrievals and are averaged on the 12×12 km^2 grid to create a characteristic averaging kernel for each super-observation. We follow the approach of Varon et al. (2022) to regrid the GEOS-Chem atmosphere to the MethaneAIR vertical grid and convolve it with the MethaneAIR averaging kernel to emulate MethaneAIR observation of the GEOS-Chem atmosphere. GEOS-Chem fields are updated hourly and matched to MethaneAIR's observation times.

Inversion of MethaneAIR observations cannot use the smoothed TROPOMI boundary conditions because the MethaneAIR observations are only for one day. Here we use the lowest MethaneAIR super-observed X_{CH4} on the 12×12 km^2 grid as our

https://doi.org/10.5194/egusphere-2025-4626
Preprint. Discussion started: 14 November 2025

best prior estimate of the boundary conditions in all four cardinal directions, with a relative vertical distribution of concentrations from the GEOS-Chem simulation. This boundary condition is applied at the edge of the inversion domain in Figure 1, extending some distance away from the MethaneAIR observation scene, so that the MethaneAIR observations can optimize emissions upwind of the scene. We optimize the boundary conditions in that inversion with a prior error standard deviation of 2 ppb. This is lower than the prior error standard deviation on the boundaries for the TROPOMI inversion because we are using a direct observational value to estimate the inflow.

The observing system error covariance matrix for MethaneAIR includes contributions from GEOS-Chem transport, instrument retrieval, and representation errors added in quadrature and with no error correlation between 12×12 km^2 grid cells (diagonal matrix). The GEOS-Chem transport error standard deviation is taken to be 5 ppb, same as for TROPOMI. The single-retrieval error standard deviation for MethaneAIR retrievals is 80 ppb but is mainly random noise (Chan Miller et al., 2024), so we expect it to drop to negligible values relative to the transport error when averaged into a super-observation (~3×10^5 individual retrievals). Representation error arises because 12×12 km^2 grid cells along the edge of the MethaneAIR viewing scene are only partly sampled by MethaneAIR. To estimate this representation error, we select all 12×12 km^2 grid cells in our dataset where there is full MethaneAIR observational coverage, successively remove data from 10% of each grid cell area and calculate the root-mean-square error (RMSE) of the resulting super-observations compared to the fully observed grid cells. From there we obtain the representation error standard deviation σ_R (ppb):

$$\sigma_R = 4.7\,(1 - C) \tag{3}$$

where C is the area fraction of the 12×12 km^2 grid cell with MethaneAIR observations.

2.4 Inversion Specifications

For each MethaneAIR flight we perform three types of inversions: (1) a MethaneAIR-only inversion which ingests the MethaneAIR observations on the flight day and optimizes emissions for that day; (2) a TROPOMI-only inversion which ingests TROPOMI observations from the month centered on the flight day and optimizes emissions for that month.; (3) a TROPOMI+MethaneAIR inversion which uses the posterior emissions generated by the TROPOMI-only base inversion as prior estimate for the MethaneAIR-only inversion. Comparison of (1) and (2) evaluates the consistency between the emissions inferred by MethaneAIR and TROPOMI. Comparison of (1) and (3) evaluates the benefit of using TROPOMI observations to inform the MethaneAIR inversion. The two-step inversion (3) effectively combines the information from TROPOMI and MethaneAIR. Concatenating the TROPOMI and MethaneAIR data into a single observation vector would not be as effective because of the different time scales over which the observations operate and the expected temporal variability of emissions.

https://doi.org/10.5194/egusphere-2025-4626
Preprint. Discussion started: 14 November 2025

We use for the inversion the default prior emission inventories at 0.1°×0.1° resolution from IMI 2.0 (Estrada et al., 2025) including the gridded US EPA Greenhouse Gas Inventory (GHGI) (Maasakkers et al., 2023). We supersede the emissions from the oil/gas sector with those from Omara et al. (2024), which include more measurement-based and facility-specific information than the GHGI Total prior emissions within the MethaneAIR flight domains are 60.0 and 13.2 t h^{-1} for the Permian scene (RF06) and the Uinta scene (RF08) respectively, dominated by the oil/gas sector. We also conduct a sensitivity inversion for the Permian scene using the GHGI oil/gas emissions instead of Omara et al. (2024) to determine the sensitivity of posterior emissions estimates to the choice of prior emissions. The GHGI prior emission total for the Permian scene is 13.8 t h^{-1}, 4-fold lower than Omara et al. (2024) and with a different spatial distribution.

The inversions optimize emissions on the 12×12 km^2 grid for the domains shown in Figure 1, resulting in 293 emission state vector elements for RF06 and 276 for RF08. There are in addition four boundary conditions state vector elements, and eight emission state vector elements for the buffer regions (TROPOMI inversion only). For RF06 we have 51 MethaneAIR super-observations and 1012 TROPOMI super-observations (2318 individual observations). For RF08 we have 48 MethaneAIR super-observations and 1474 TROPOMI super-observations (1737 individual observations). The TROPOMI super-observations average only a small number of individual observations. The mean observing system error standard deviations are 5.1 ppb for MethaneAIR and 13.8 ppb for TROPOMI.

https://doi.org/10.5194/egusphere-2025-4626
Preprint. Discussion started: 14 November 2025

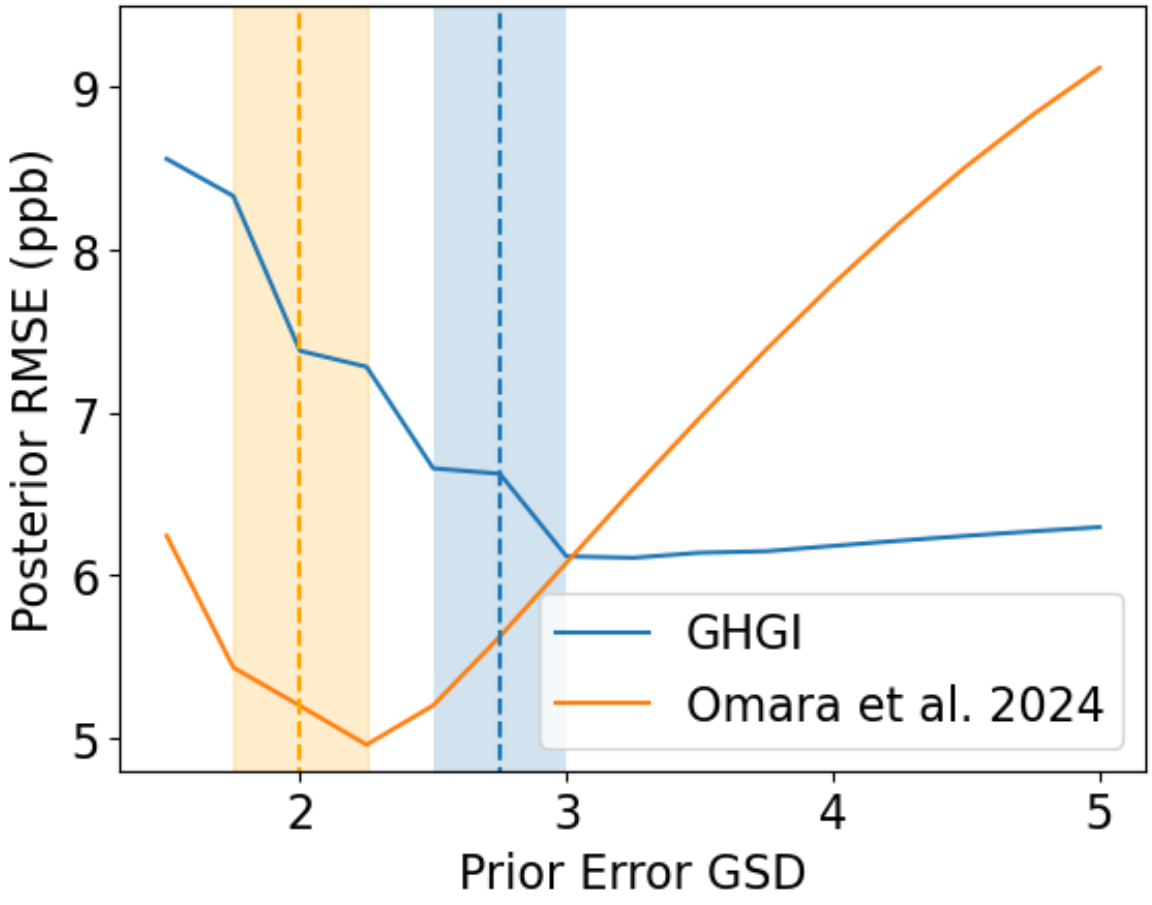

Figure 2: Selection of the geometric standard deviation (GSD) of the lognormal error PDF for the prior emissions used in the inversion. The Figure shows the RMSE of modeled X_{CH4} with posterior emissions compared to the MethaneAIR observations, plotted as a function of the GSD for either the Omara et al. (2024) or EPA Greenhouse Gas Inventory (GHGI) taken as the prior estimate. Dashed lines indicate the GSD values selected for our base inversion and shadings indicate the ranges for the inversion ensemble.

We conduct a base inversion using our best estimates of inversion parameters, and an inversion ensemble varying these parameters within their expected ranges to characterize the uncertainty in our results. This is a more conservative estimate of the uncertainty than the posterior error covariance matrix (Chen et al., 2022). The geometric standard deviation of (GSD) of the lognormal error PDF for the prior emission estimate is a particularly important parameter, and we select it as shown in Figure 2 on the basis of the resulting RMSE of the GEOS-Chem simulation with posterior emissions compared to MethaneAIR observations. A low prior error GSD does not allow the inversion to fit the observations, but an excessively high prior error GSD prevents regularization of the solution, particularly when using a high-quality prior estimate as with Omara et al. (2024). There results a minimum in the RMSE vs. GSD relationship that guides the choice of an optimal GSD for the MethaneAIR inversions. To avoid sampling the rising branch where the inversion would increase the RMSE, we choose a GSD of 2 for the

https://doi.org/10.5194/egusphere-2025-4626
Preprint. Discussion started: 14 November 2025

Omara et al. (2024) prior estimate in the base inversion, with a range of 1.75 to 2.25 for the inversion ensemble. We choose a GSD of 2.75 for the GHGI prior estimate in the base inversion, with a range of 2.5 to 3.0 for the inversion ensemble. For the TROPOMI inversions we use GSD of 2 with a range of 1.75 to 2.25 for both cases. For the error standard deviation on the MethaneAIR boundary conditions we use a best estimate of 2 ppb and an ensemble range of 1 to 3 ppb. For the error standard deviation on the TROPOMI boundary conditions we use a best estimate of 10 ppb and an ensemble range of 5 to 15 ppb. For each inversion type we thus have eight ensemble members in addition to the base inversion.

3 Results and Discussion

3.1 Permian Scene (RF06)

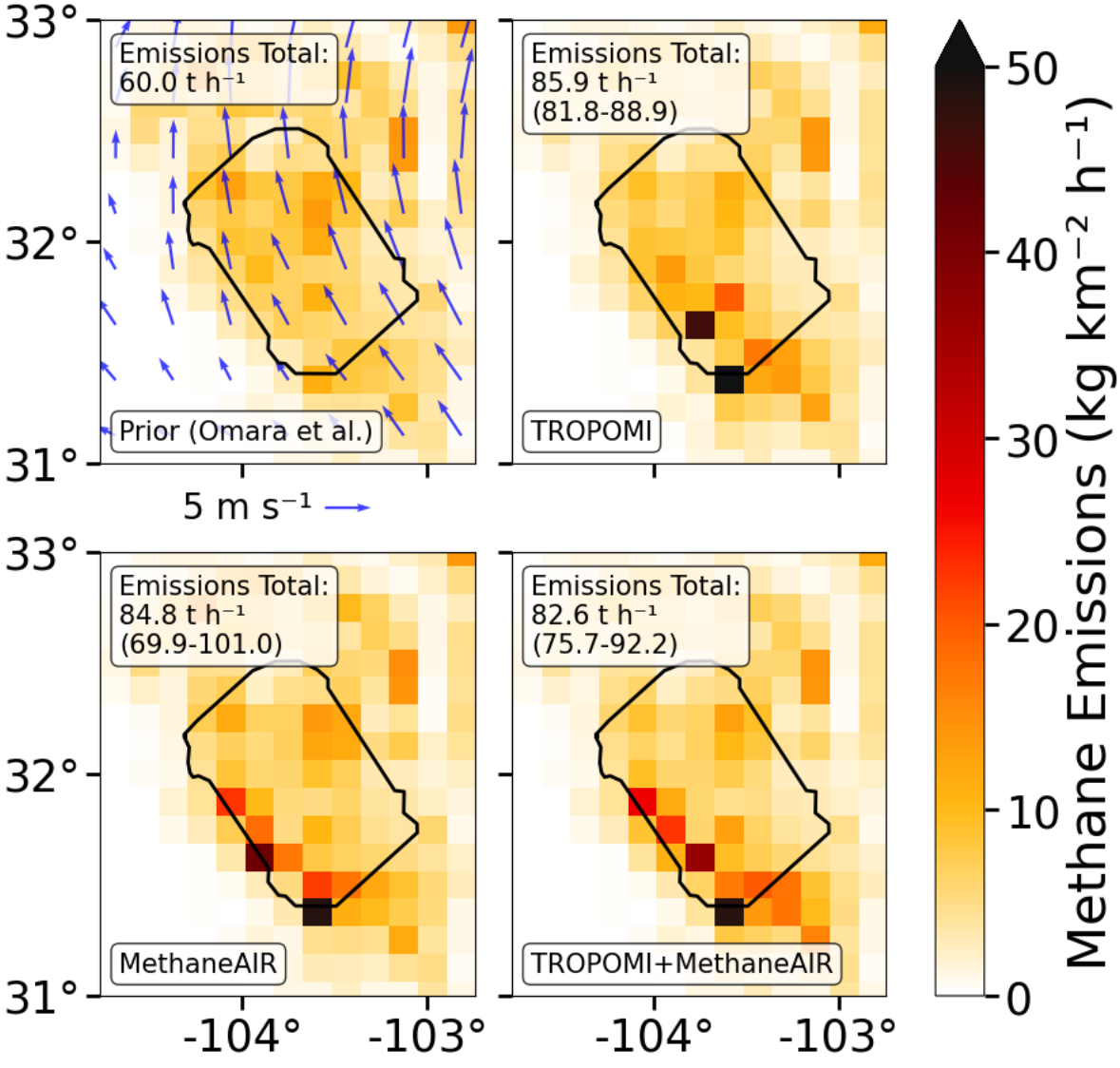

https://doi.org/10.5194/egusphere-2025-4626
Preprint. Discussion started: 14 November 2025

Figure 3: Methane emissions in the Delaware section of the Permian Basin plotted on the 12×12 km^2 grid of the Integrated Methane Inversion (IMI), with the MethaneAIR RF06 flight domain on August 8, 2021, delineated as black line. The top left panel shows the prior estimate including oil and gas emissions from Omara et al. (2024). Blue arrows indicate the GEOS-FP 70-m altitude winds for the MethaneAIR flight period. Other panels show posterior emission estimates for the inversions using MethaneAIR observations (lower left), TROPOMI observations (upper right), and MethaneAIR observations with the TROPOMI posterior estimate as prior estimate (lower right). Emission totals for the MethaneAIR flight domain are given inset, with ranges from the inversion ensemble given in parentheses. Emissions in grid cells on the border of the flight domain are attributed to the flight domain in proportion to their fractional areas within the domain.

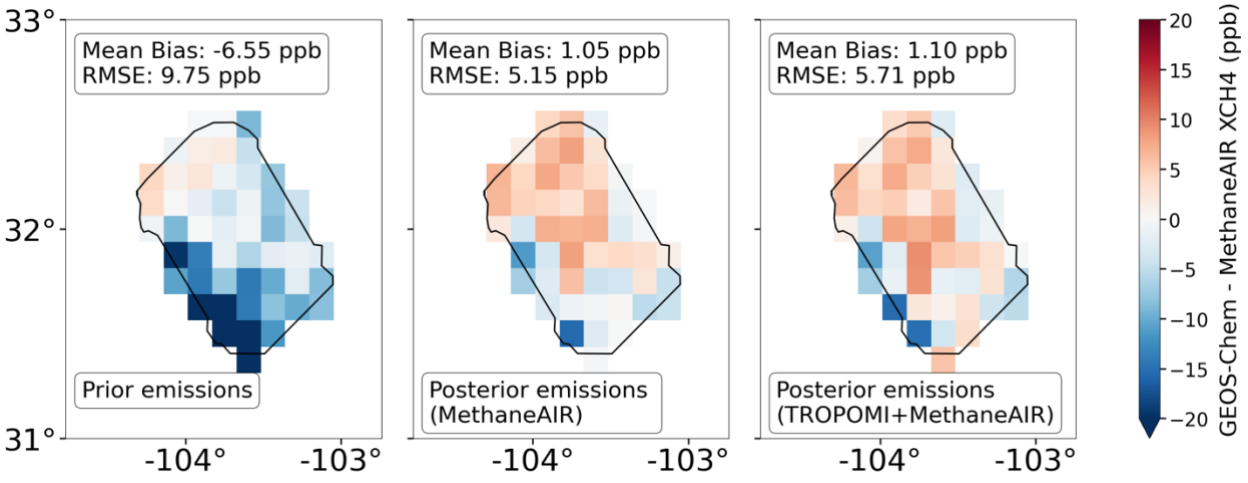

Figure 4: Difference between GEOS-Chem simulations and MethaneAIR X_{CH4} observations for RF06 over the Permian Basin. GEOS-Chem simulations are driven by prior emissions (left panel), posterior MethaneAIR emissions (middle panel), and posterior TROPOMI+MethaneAIR emissions (right panel). Mean bias and RMSE are given inset.

Figure 3 shows the prior and posterior emission estimates for the Permian MethaneAIR flight on August 8, 2021(RF06), and Figure 4 shows X_{CH4} differences between GEOS-Chem simulations driven by these emissions and the MethaneAIR observations. The simulation with prior emissions from Omara et al. (2024), totaling 60 t h^{-1} in the MethaneAIR flight domain, is biased low compared to the observations. The three inversions correct that bias by increasing emissions to 83-86 t h^{-1}. RMSEs are also improved from 9.8 ppb to 5.2-5.7 ppb. Previous inversions of TROPOMI observations found emissions in the same domain of 80-100 t h^{-1} (Zhang et al., 2020; Cusworth et al., 2022; Varon et al., 2023). Winds for the MethaneAIR flight period were south-easterly, with significant emissions upwind from the flight domain but within the inversion domain. The inversion corrects those upwind emissions as well, moderating the increase of emissions within the flight domain.

https://doi.org/10.5194/egusphere-2025-4626
Preprint. Discussion started: 14 November 2025

The MethaneAIR and TROPOMI inversions, driven by independent observations, show remarkable consistency in their posterior emissions, totalling 85 t h^{-1} in the MethaneAIR inversion and 86 t h^{-1} in the TROPOMI inversion. MethaneAIR generates a series of hotspots along the southwestern portion of the flight domain, with the largest being at the southern tip of the flight domain, none of which were present in the prior estimate. The TROPOMI inversion reproduces the largest hotspot on the southern tip and places another hotspot at a location adjacent to a MethaneAIR inversion hotspot. It does not capture the others. The inversions are for a month (TROPOMI) versus a single day (MethaneAIR), and temporal variability of emissions could be a factor in the difference of spatial distributions. The locations of the emission hotspots are upwind of where the highest concentrations are observed (Figure 1), stressing the importance of transport in the inversion results.

The TROPOMI+MethaneAIR inversion, using posterior emissions from TROPOMI as prior estimates for the MethaneAIR inversion, shows a total posterior emission within the flight domain of 83 (76-92) t h^{-1}, where the parentheses indicate the uncertainty diagnosed by the spread in the inversion ensemble. This is consistent with the MethaneAIR inversion result of 85 (70-101) t h^{-1} but narrows the uncertainty. It does not improve on the fit to the MethaneAIR observations (Figure 3), but it does not degrade it significantly either. It relocates one of the hotspots to the location identified by the TROPOMI-only inversion and is more consistent with where MethaneAIR observes a concentration hotspot (Figure 1).

https://doi.org/10.5194/egusphere-2025-4626
Preprint. Discussion started: 14 November 2025

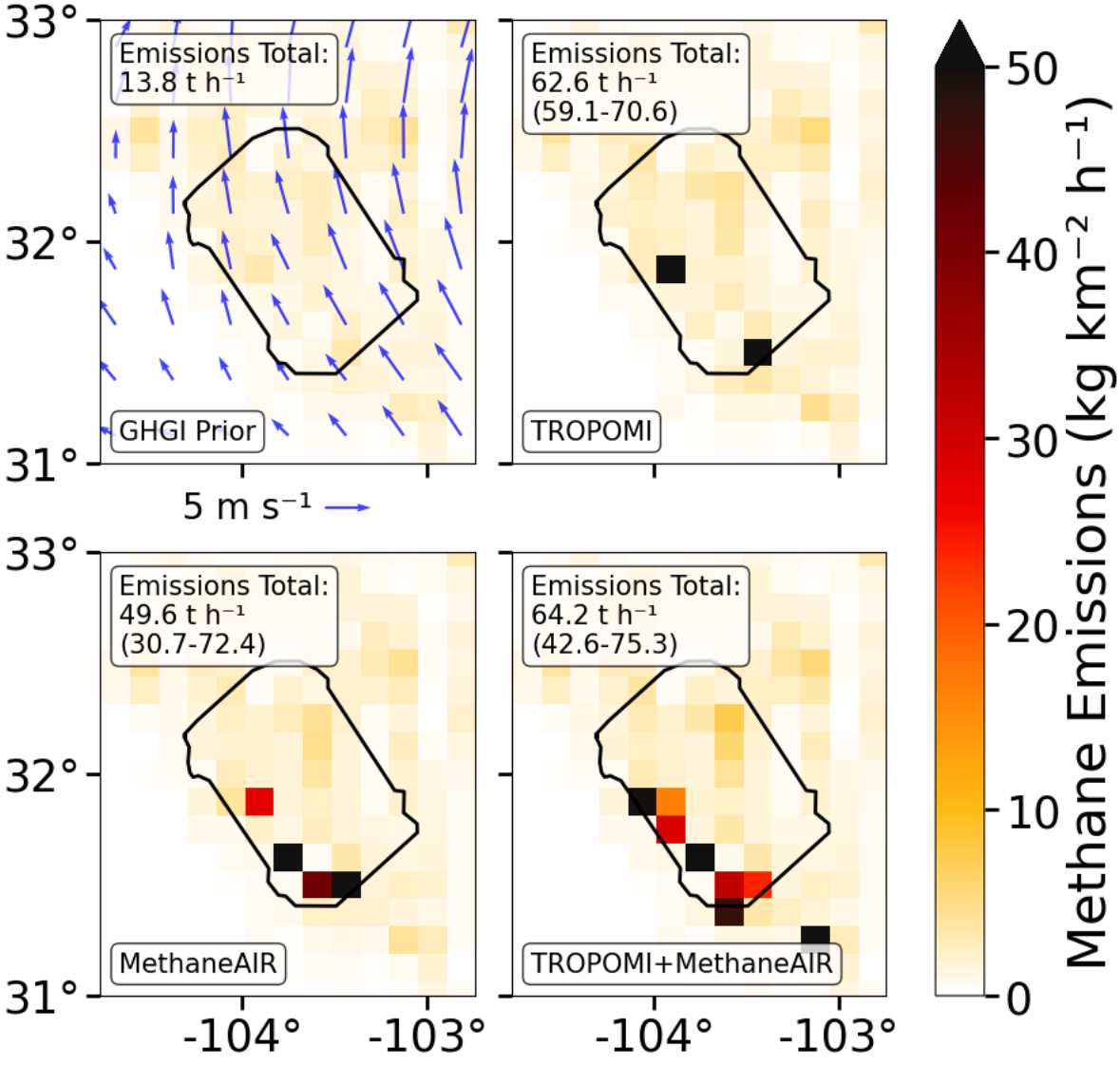

Figure 5: Same as Figure 3 but using GHGI as prior estimate for oil and gas emissions instead of Omara et al. (2024).

https://doi.org/10.5194/egusphere-2025-4626
Preprint. Discussion started: 14 November 2025

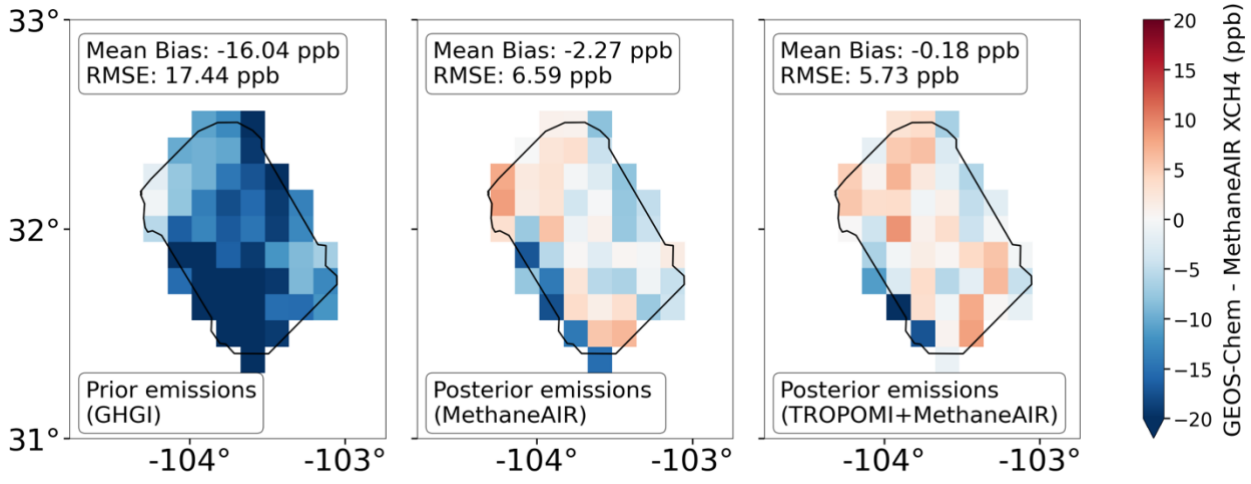

Figure 6: Same as Figure 4 but using GHGI as prior estimate for oil and gas emissions instead of Omara et al. (2024).

.

Figure 5 shows the prior and posterior emission estimates using GHGI as prior estimate for oil and gas emissions instead of Omara et al. (2024), and Figure 6 shows X_{CH4} differences between GEOS-Chem simulations driven by these emissions and the MethaneAIR observations. The GHGI emissions totaling 14 t h^{-1} are 4× lower than Omara et al. (2024), and the inversion strongly corrects this, yielding posterior emission totals of 63-64 t h^{-1}. The posterior emissions are lower than with the Omara et al. (2024) prior estimate because the prior estimate contributes information to the solution, as it should, but the higher prior error GSD for the GHGI (Figure 2) enables stronger corrections. Correction of the spatial distribution of emissions places hotspots in the south and southwestern edges of the flight domain, as with the Omara et al. (2024) prior estimate, but the locations are not precisely the same (compare to Figure 3) and this can be attributed to ineffective regularization from the GHGI. The MethaneAIR+TROPOMI inversion is much better at reproducing the spatial distribution and this can be attributed to the additional information from TROPOMI. We see that prior information from TROPOMI is more important in guiding the MethaneAIR inversion when the original bottom-up prior information is poorer.

3.2 Uinta Scene (RF08)

https://doi.org/10.5194/egusphere-2025-4626
Preprint. Discussion started: 14 November 2025

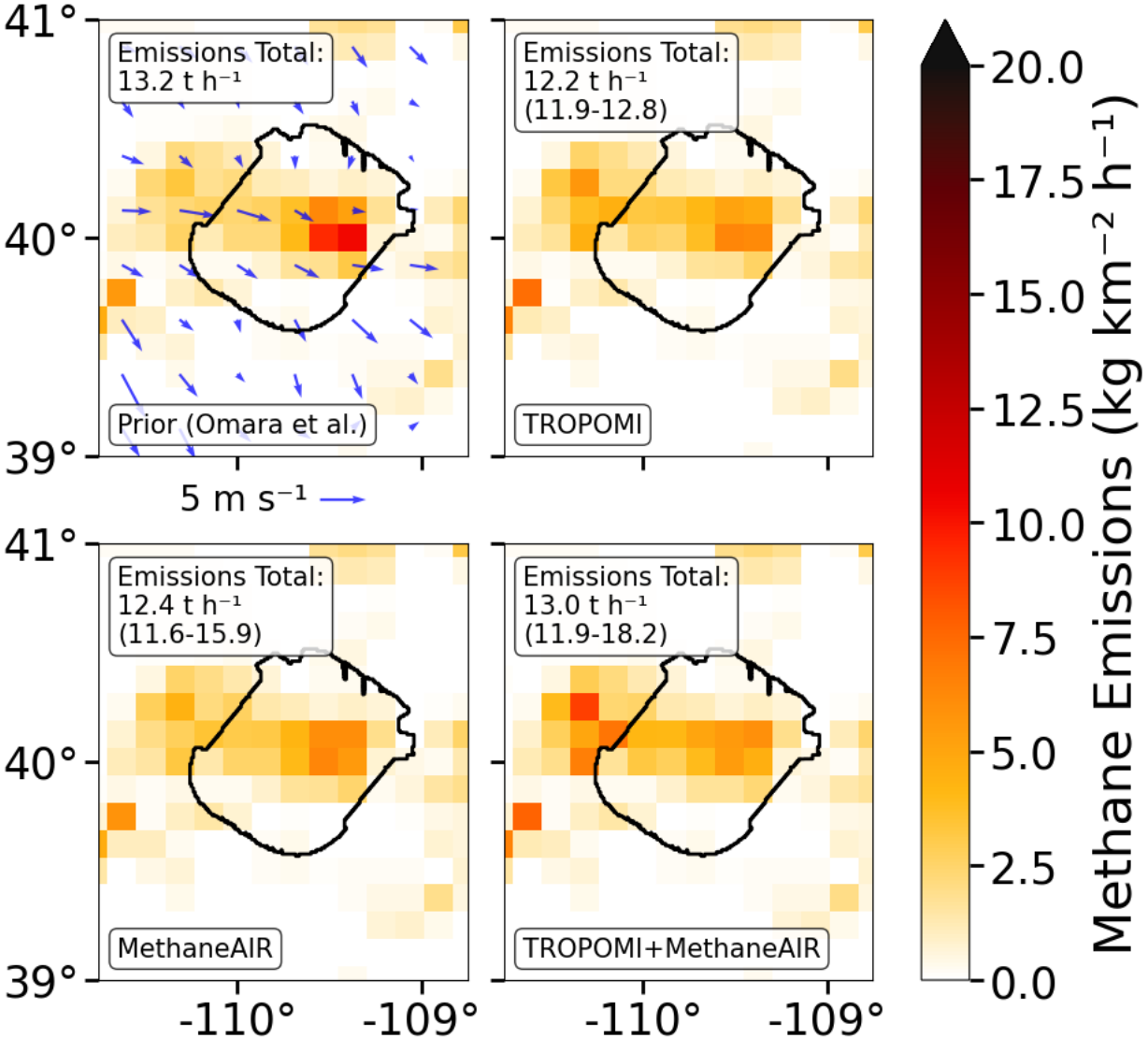

Figure 7: Same as Figure 3 but for the Uinta Basin on August 11, 2021.

https://doi.org/10.5194/egusphere-2025-4626
Preprint. Discussion started: 14 November 2025

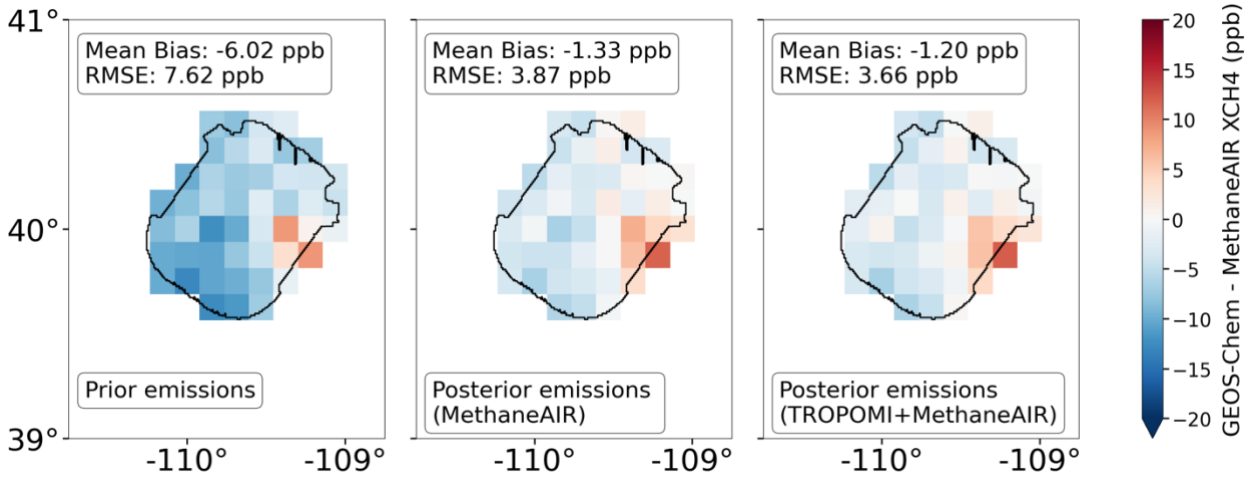

Figure 8: Same as Figure 4 but for the Uinta Basin on August 11, 2021.

Figure 7 shows the prior and posterior emission estimates for the Uinta (RF08) flight domain on August 11, 2021, and Figure 8 shows the differences of the corresponding GEOS-Chem simulations with the MethaneAIR observations. The X_{CH4} enhancements are much weaker than in the Permian (Figure 1) and the emissions are correspondingly weaker. The flow is prevailing westerly but is more complicated than in the Permian, reflecting the topography in the region. The prior estimates from Omara et al. (2024) are more localized than in the Permian. These three factors make for a more challenging inversion. TROPOMI observations are further limited in the mountainous areas surrounding the Basin.

The GEOS-Chem simulation with the Omara et al. (2024) prior emissions, totaling 13 t h^{-1} for the MethaneAIR flight domain, is biased low by 6.0 ppb relative to the MethaneAIR observations with an RMSE of 7.6 ppb. The MethaneAIR inversion reduces the bias to 1.3 ppb and improves the RMSE to 3.9 ppb even though it reduces total emissions slightly to 12 t h^{-1}. It does so by shifting emissions upwind to the west. The TROPOMI inversion results are again remarkably consistent considering that the observations are completely independent.

The TROPOMI+MethaneAIR inversion, using results from the TROPOMI inversion as prior estimate for the MethaneAIR inversion, is closely consistent with the other inversions in terms of total emissions and their spatial distribution. It further improves on the bias relative to the MethaneAIR observations, down to 0.8 ppb, with an RMSE of 3.6 ppb. It places the largest emissions upwind of the flight domain, supporting the prior information from TROPOMI. It shows a larger spread in the inversion ensemble, reflecting variations in emissions from grid cells along the western edge of the flight domain.

4 Conclusions

https://doi.org/10.5194/egusphere-2025-4626
Preprint. Discussion started: 14 November 2025

We have shown that TROPOMI satellite and MethaneAIR aircraft observations of atmospheric methane over oil/gas production fields can be ingested into a common Integrated Methane Inversion (IMI) framework for improved quantification of methane emissions. The new capability for the IMI to ingest MethaneAIR observations will next be applied to the MethaneSAT satellite instrument for which MethaneAIR is the aircraft emulator.

MethaneAIR provides highly precise but single-day observations over ~100×100 km^2 scenes while TROPOMI provides continuous but sparser and coarser observations. The IMI was originally designed for TROPOMI inversions, and we adapted it to perform MethaneAIR inversions with 12×12 km^2 resolution and lognormal error probability density functions (PDFs) on prior emission estimates to improve spatialization. We showed how the geometric standard deviation (GSD) for the prior error PDF can be optimized by using the root-mean-square error (RMSE) in the fit to observations, with lower GSD when higher-quality prior information is available. Comparisons of independent MethaneAIR (single day) and TROPOMI (monthly) inversions within the IMI show remarkable consistency as well as some differences that may be investigated in terms of temporal variability of emissions. Using TROPOMI inversion results as prior estimates for MethaneAIR inversions significantly improves MethaneAIR inversion results by correcting emissions upwind of the observation scene and adding to the prior information, particularly when the quality of the prior estimates is low or when observed concentration gradients are weak. We find that the IMI is able to improve emissions estimates even when starting from a very poor prior estimate.

There are some issues for which further study is warranted as we proceed to apply the IMI to the collection of MethaneSAT observation scenes. Log-normal error PDFs on prior estimates of varying reliability require custom GSDs and the optimization of these GSDs should be automated as part of the IMI. Discrepancies between results from TROPOMI and MethaneSAT inversions should be investigated in terms of temporal variability of emissions and/or unrecognized biases in the inversions. Having multiple MethaneSAT observations of the same scene on different days will help. Optimization of boundary conditions for the MethaneSAT scenes could be improved by using GEOS-Chem applied to the posterior TROPOMI solution for the sources upwind. As new methane observations from the recently launched Sentinel-5 satellite become available, providing a dataset comparable but denser to TROPOMI (Jacob et al., 2022), they should be integrated as an additional resource to support MethaneSAT inversions. Together with the inclusion of point source observations (Estrada et al., 2025), the IMI will become in this manner a common consistent platform for the inversion of multi-scale multi-instrument satellite datasets.

Data/Code Availability

The IMI is open source and can all code for it can be accessed at https://github.com/geoschem/integrated_methane_inversion. L2 MethaneAIR data used in this work are available through Google Drive https://drive.google.com/drive/folders/1wketmNNUKWEdVUVHU-WB87hIE4rO1Ce_?usp=drive_link. Blended TROPOMI+GOSAT data is available through the Harvard Dataverse portal at https://dataverse.harvard.edu/dataverse/blended-tropomi-gosat-methane. GEOS-FP meteorology files at 12 km resolution are

https://doi.org/10.5194/egusphere-2025-4626
Preprint. Discussion started: 14 November 2025

available through Washington University at http://geoschemdata.wustl.edu/ExtData/GEOS_0.125x0.15625_NA/GEOS_FP_DerivedWinds/.

370

Author Contributions

JB performed the primary data analysis and inversion calculations; XW and MP developed the 12 km IMI capability, XW, MP, and LE provided technical support; DJ and RG advised the project; JB and DJ wrote the manuscript draft; XW, MP, LA, DV, SW, MO, and RG reviewed and edited the manuscript.

375

Competing Interests

The authors declare that they have no conflict of interest.

Acknowledgements

380 This work was funded by the Environmental Defence Fund. GEOS-Chem input files were obtained from the GEOS-Chem Data Portal enabled by Washington University.

References

Baray, S., Vogel, F. R., Varon, D. J., Estrada, L., Balasus, N., Jones, D. B. A., McLinden, C. A., Griffin, D., Duren, R., and Cusworth, D.: Monitoring methane emissions in Western Canada from space using a constellation of satellites: TROPOMI, 385 GOSAT-1/2, GHGSat, and Carbon Mapper, 2023, A42F-05, 2023.

Chan Miller, C., Roche, S., Wilzewski, J. S., Liu, X., Chance, K., Souri, A. H., Conway, E., Luo, B., Samra, J., Hawthorne, J., Sun, K., Staebell, C., Chulakadabba, A., Sargent, M., Benmergui, J. S., Franklin, J. E., Daube, B. C., Li, Y., Laughner, J. L., Baier, B. C., Gautam, R., Omara, M., and Wofsy, S. C.: Methane retrieval from MethaneAIR using the CO_2 proxy approach: 390 a demonstration for the upcoming MethaneSAT mission, Atmospheric Measurement Techniques, 17, 5429–5454, https://doi.org/10.5194/amt-17-5429-2024, 2024.

Chen, Z., Jacob, D. J., Nesser, H., Sulprizio, M. P., Lorente, A., Varon, D. J., Lu, X., Shen, L., Qu, Z., Penn, E., and Yu, X.: Methane emissions from China: a high-resolution inversion of TROPOMI satellite observations, Atmospheric Chemistry and 395 Physics, 22, 10809–10826, https://doi.org/10.5194/acp-22-10809-2022, 2022.

Chen, Z., Jacob, D. J., Gautam, R., Omara, M., Stavins, R. N., Stowe, R. C., Nesser, H., Sulprizio, M. P., Lorente, A., Varon, D. J., Lu, X., Shen, L., Qu, Z., Pendergrass, D. C., and Hancock, S.: Satellite quantification of methane emissions and oil–gas

https://doi.org/10.5194/egusphere-2025-4626
Preprint. Discussion started: 14 November 2025

methane intensities from individual countries in the Middle East and North Africa: implications for climate action, Atmospheric Chemistry and Physics, 23, 5945–5967, https://doi.org/10.5194/acp-23-5945-2023, 2023.

Chulakadabba, A., Sargent, M., Lauvaux, T., Benmergui, J. S., Franklin, J. E., Chan Miller, C., Wilzewski, J. S., Roche, S., Conway, E., Souri, A. H., Sun, K., Luo, B., Hawthrone, J., Samra, J., Daube, B. C., Liu, X., Chance, K., Li, Y., Gautam, R., Omara, M., Rutherford, J. S., Sherwin, E. D., Brandt, A., and Wofsy, S. C.: Methane point source quantification using MethaneAIR: a new airborne imaging spectrometer, Atmospheric Measurement Techniques, 16, 5771–5785, https://doi.org/10.5194/amt-16-5771-2023, 2023.

Cusworth, D. H., Thorpe, A. K., Ayasse, A. K., Stepp, D., Heckler, J., Asner, G. P., Miller, C. E., Yadav, V., Chapman, J. W., Eastwood, M. L., Green, R. O., Hmiel, B., Lyon, D. R., and Duren, R. M.: Strong methane point sources contribute a disproportionate fraction of total emissions across multiple basins in the United States, Proceedings of the National Academy of Sciences, 119, e2202338119, https://doi.org/10.1073/pnas.2202338119, 2022.

Eskes, H. J., Velthoven, P. F. J. V., Valks, P. J. M., and Kelder, H. M.: Assimilation of GOME total-ozone satellite observations in a three-dimensional tracer-transport model, Q. J. Roy. Meteor. Soc., 129, 1663–1681, https://doi.org/10.1256/qj.02.14, 2003.

Estrada, L. A., Varon, D. J., Sulprizio, M., Nesser, H., Chen, Z., Balasus, N., Hancock, S. E., He, M., East, J. D., Mooring, T. A., Oort Alonso, A., Maasakkers, J. D., Aben, I., Baray, S., Bowman, K. W., Worden, J. R., Cardoso-Saldaña, F. J., Reidy, E., and Jacob, D. J.: Integrated Methane Inversion (IMI) 2.0: an improved research and stakeholder tool for monitoring total methane emissions with high resolution worldwide using TROPOMI satellite observations, Geoscientific Model Development, 18, 3311–3330, https://doi.org/10.5194/gmd-18-3311-2025, 2025.

Frankenberg, C., Meirink, J. F., van Weele, M., Platt, U., and Wagner, T.: Assessing Methane Emissions from Global Space-Borne Observations, Science, 308, 1010–1014, https://doi.org/10.1126/science.1106644, 2005.

Hancock, S. E., Jacob, D. J., Chen, Z., Nesser, H., Davitt, A., Varon, D. J., Sulprizio, M. P., Balasus, N., Estrada, L. A., Cazorla, M., Dawidowski, L., Diez, S., East, J. D., Penn, E., Randles, C. A., Worden, J., Aben, I., Parker, R. J., and Maasakkers, J. D.: Satellite quantification of methane emissions from South American countries: a high-resolution inversion of TROPOMI and GOSAT observations, Atmospheric Chemistry and Physics, 25, 797–817, https://doi.org/10.5194/acp-25-797-2025, 2025.

https://doi.org/10.5194/egusphere-2025-4626
Preprint. Discussion started: 14 November 2025

Heald, C. L., Jacob, D. J., Jones, D. B. A., Palmer, P. I., Logan, J. A.,Streets, D. G., Sachse, G. W., Gille, J. C., Hoffman, R. N., and Nehrkorn, T.: Comparative inverse analysis of satellite (MOPITT) and aircraft (TRACE-P) observations to estimate Asian sources of carbon monoxide, J. Geophys. Res.-Atmos., 109,D23306, https://doi.org/10.1029/2004JD005185, 2004.

Hemati, M., Mahdianpari, M., Nassar, R., Shiri, H., and Mohammadimanesh, F.: Urban methane emission monitoring across North America using TROPOMI data: an analytical inversion approach, Sci Rep, 14, 9041, https://doi.org/10.1038/s41598-024-58995-8, 2024.

Jacob, D. J., Varon, D. J., Cusworth, D. H., Dennison, P. E., Frankenberg, C., Gautam, R., Guanter, L., Kelley, J., McKeever, J., Ott, L. E., Poulter, B., Qu, Z., Thorpe, A. K., Worden, J. R., and Duren, R. M.: Quantifying methane emissions from the global scale down to point sources using satellite observations of atmospheric methane, Atmospheric Chemistry and Physics, 22, 9617–9646, https://doi.org/10.5194/acp-22-9617-2022, 2022.

Krings, T., Gerilowski, K., Buchwitz, M., Reuter, M., Tretner, A., Erzinger, J., Heinze, D., Pflüger, U., Burrows, J. P., and Bovensmann, H.: MAMAP – a new spectrometer system for column-averaged methane and carbon dioxide observations from aircraft: retrieval algorithm and first inversions for point source emission rates, Atmospheric Measurement Techniques, 4, 1735–1758, https://doi.org/10.5194/amt-4-1735-2011, 2011.

Laughner, J. L., Toon, G. C., Mendonca, J., Petri, C., Roche, S., Wunch, D., Blavier, J.-F., Griffith, D. W. T., Heikkinen, P., Keeling, R. F., Kiel, M., Kivi, R., Roehl, C. M., Stephens, B. B., Baier, B. C., Chen, H., Choi, Y., Deutscher, N. M., DiGangi, J. P., Gross, J., Herkommer, B., Jeseck, P., Laemmel, T., Lan, X., McGee, E., McKain, K., Miller, J., Morino, I., Notholt, J., Ohyama, H., Pollard, D. F., Rettinger, M., Riris, H., Rousogenous, C., Sha, M. K., Shiomi, K., Strong, K., Sussmann, R., Té, Y., Velazco, V. A., Wofsy, S. C., Zhou, M., and Wennberg, P. O.: The Total Carbon Column Observing Network's GGG2020 data version, Earth System Science Data, 16, 2197–2260, https://doi.org/10.5194/essd-16-2197-2024, 2024.

Liang, R., Zhang, Y., Chen, W., Zhang, P., Liu, J., Chen, C., Mao, H., Shen, G., Qu, Z., Chen, Z., Zhou, M., Wang, P., Parker, R. J., Boesch, H., Lorente, A., Maasakkers, J. D., and Aben, I.: East Asian methane emissions inferred from high-resolution inversions of GOSAT and TROPOMI observations: a comparative and evaluative analysis, Atmospheric Chemistry and Physics, 23, 8039–8057, https://doi.org/10.5194/acp-23-8039-2023, 2023.

Lorente, A., Borsdorff, T., Butz, A., Hasekamp, O., aan de Brugh, J., Schneider, A., Wu, L., Hase, F., Kivi, R., Wunch, D., Pollard, D. F., Shiomi, K., Deutscher, N. M., Velazco, V. A., Roehl, C. M., Wennberg, P. O., Warneke, T., and Landgraf, J.: Methane retrieved from TROPOMI: improvement of the data product and validation of the first 2 years of measurements, Atmospheric Measurement Techniques, 14, 665–684, https://doi.org/10.5194/amt-14-665-2021, 2021.

https://doi.org/10.5194/egusphere-2025-4626
Preprint. Discussion started: 14 November 2025

Lu, X., Jacob, D. J., Zhang, Y., Maasakkers, J. D., Sulprizio, M. P., Shen, L., Qu, Z., Scarpelli, T. R., Nesser, H., Yantosca, R. M., Sheng, J., Andrews, A., Parker, R. J., Boesch, H., Bloom, A. A., and Ma, S.: Global methane budget and trend, 2010–2017: complementarity of inverse analyses using in situ (GLOBALVIEWplus CH_4 ObsPack) and satellite (GOSAT) observations, Atmospheric Chemistry and Physics, 21, 4637–4657, https://doi.org/10.5194/acp-21-4637-2021, 2021.

Lyon, D. R., Zavala-Araiza, D., Alvarez, R. A., Harriss, R., Palacios, V., Lan, X., Talbot, R., Lavoie, T., Shepson, P., Yacovitch, T. I., Herndon, S. C., Marchese, A. J., Zimmerle, D., Robinson, A. L., and Hamburg, S. P.: Constructing a Spatially Resolved Methane Emission Inventory for the Barnett Shale Region, Environ. Sci. Technol., 49, 8147–8157, https://doi.org/10.1021/es506359c, 2015.

Maasakkers, J. D., Jacob, D. J., Sulprizio, M. P., Scarpelli, T. R., Nesser, H., Sheng, J.-X., Zhang, Y., Hersher, M., Bloom, A. A., Bowman, K. W., Worden, J. R., Janssens-Maenhout, G., and Parker, R. J.: Global distribution of methane emissions, emission trends, and OH concentrations and trends inferred from an inversion of GOSAT satellite data for 2010–2015, Atmospheric Chemistry and Physics, 19, 7859–7881, https://doi.org/10.5194/acp-19-7859-2019, 2019.

Maasakkers, J. D., McDuffie, E. E., Sulprizio, M. P., Chen, C., Schultz, M., Brunelle, L., Thrush, R., Steller, J., Sherry, C., Jacob, D. J., Jeong, S., Irving, B., and Weitz, M.: A Gridded Inventory of Annual 2012–2018 U.S. Anthropogenic Methane Emissions, Environ. Sci. Technol., 57, 16276–16288, https://doi.org/10.1021/acs.est.3c05138, 2023.

Miura, T., Inaoka, K., Kachi, M., and Kojima, Y.: Overview and current status of GOSAT-GW mission and AMSR3 instrument, in: Sensors, Systems, and Next-Generation Satellites XXVII, Sensors, Systems, and Next-Generation Satellites XXVII, 83–88, https://doi.org/10.1117/12.2678886, 2023.

Nathan, B., Maasakkers, J. D., Naus, S., Gautam, R., Omara, M., Varon, D. J., Sulprizio, M. P., Estrada, L. A., Lorente, A., Borsdorff, T., Parker, R. J., and Aben, I.: Assessing methane emissions from collapsing Venezuelan oil production using TROPOMI, Atmospheric Chemistry and Physics, 24, 6845–6863, https://doi.org/10.5194/acp-24-6845-2024, 2024.

Omara, M., Himmelberger, A., MacKay, K., Williams, J. P., Benmergui, J., Sargent, M., Wofsy, S. C., and Gautam, R.: Constructing a measurement-based spatially explicit inventory of US oil and gas methane emissions (2021), Earth System Science Data, 16, 3973–3991, https://doi.org/10.5194/essd-16-3973-2024, 2024.

Qu, Z., Jacob, D. J., Shen, L., Lu, X., Zhang, Y., Scarpelli, T. R., Nesser, H., Sulprizio, M. P., Maasakkers, J. D., Bloom, A. A., Worden, J. R., Parker, R. J., and Delgado, A. L.: Global distribution of methane emissions: a comparative inverse analysis

https://doi.org/10.5194/egusphere-2025-4626
Preprint. Discussion started: 14 November 2025

of observations from the TROPOMI and GOSAT satellite instruments, Atmospheric Chemistry and Physics, 21, 14159–14175, https://doi.org/10.5194/acp-21-14159-2021, 2021.

Riddick, S. N., Mbua, M., Santos, A., Hartzell, W., and Zimmerle, D. J.: Potential Underestimate in Reported Bottom-up Methane Emissions from Oil and Gas Operations in the Delaware Basin, Atmosphere, 15, 202, https://doi.org/10.3390/atmos15020202, 2024.

Shen, L., Zavala-Araiza, D., Gautam, R., Omara, M., Scarpelli, T., Sheng, J., Sulprizio, M. P., Zhuang, J., Zhang, Y., Qu, Z., Lu, X., Hamburg, S. P., and Jacob, D. J.: Unravelling a large methane emission discrepancy in Mexico using satellite observations, Remote Sensing of Environment, 260, 112461, https://doi.org/10.1016/j.rse.2021.112461, 2021.

Shen, L., Jacob, D. J., Gautam, R., Omara, M., Scarpelli, T. R., Lorente, A., Zavala-Araiza, D., Lu, X., Chen, Z., and Lin, J.: National quantifications of methane emissions from fuel exploitation using high resolution inversions of satellite observations, Nat Commun, 14, 4948, https://doi.org/10.1038/s41467-023-40671-6, 2023.

Szopa, S., Naik, V., Adhikary, B., Artaxo, P., Berntsen, T., Collins, W. D., Fuzzi, S., Gallardo, L., Kiendler-Scharr, A., Klimont, Z., Liao, H., Unger, N., and Zanis, P.: Short-Lived Climate Forcers (Chapter 6), edited by: Masson-Delmotte, V., Zhai, P., Pirani, A., Connors, S. L., Péan, C., Berger, S., Caud, N., Chen, Y., Goldfarb, L., Gomis, M. I., Huang, M., Leitzell, K., Lonnoy, E., Matthews, J. B. R., Maycock, T. K., Waterfield, T., Yelekçi, K., Yu, R., and Zhu, B., Cambridge University Press, Cambridge, United Kingdom and New York, NY, USA, 817–922, 2021.

Varon, D. J., Jacob, D. J., Sulprizio, M., Estrada, L. A., Downs, W. B., Shen, L., Hancock, S. E., Nesser, H., Qu, Z., Penn, E., Chen, Z., Lu, X., Lorente, A., Tewari, A., and Randles, C. A.: Integrated Methane Inversion (IMI 1.0): a user-friendly, cloud-based facility for inferring high-resolution methane emissions from TROPOMI satellite observations, Geoscientific Model Development, 15, 5787–5805, https://doi.org/10.5194/gmd-15-5787-2022, 2022.

Varon, D. J., Jacob, D. J., Hmiel, B., Gautam, R., Lyon, D. R., Omara, M., Sulprizio, M., Shen, L., Pendergrass, D., Nesser, H., Qu, Z., Barkley, Z. R., Miles, N. L., Richardson, S. J., Davis, K. J., Pandey, S., Lu, X., Lorente, A., Borsdorff, T., Maasakkers, J. D., and Aben, I.: Continuous weekly monitoring of methane emissions from the Permian Basin by inversion of TROPOMI satellite observations, Atmospheric Chemistry and Physics, 23, 7503–7520, https://doi.org/10.5194/acp-23-7503-2023, 2023.

https://doi.org/10.5194/egusphere-2025-4626
Preprint. Discussion started: 14 November 2025

Wang, X., Jacob, D. J., Nesser, H., Balasus, N., Estrada, L., Sulprizio, M., Cusworth, D. H., Scarpelli, T. R., Chen, Z., East, J. D., and Varon, D. J.: Quantifying urban and landfill methane emissions in the United States using TROPOMI satellite data, https://doi.org/10.48550/arXiv.2505.10835, 16 May 2025.

Zhang, Y., Gautam, R., Pandey, S., Omara, M., Maasakkers, J. D., Sadavarte, P., Lyon, D., Nesser, H., Sulprizio, M. P., Varon, D. J., Zhang, R., Houweling, S., Zavala-Araiza, D., Alvarez, R. A., Lorente, A., Hamburg, S. P., Aben, I., and Jacob, D. J.: Quantifying methane emissions from the largest oil-producing basin in the United States from space, Science Advances, 6, eaaz5120, https://doi.org/10.1126/sciadv.aaz5120, 2020.